ORNL/SPR-2024/3535
M4LW-24OR0402029

Light Water Reactor Sustainability Program

Analysis of Deformation and Fracture Mechanisms in Friction Stir Welding Performed on Neutron-Irradiated 304 L Stainless Steel

Soyoung Kang
Wei Tang
Xiang (Frank) Chen
Maxim Gussev

August 2024

U.S. Department of Energy
Office of Nuclear Energy

ORNL/SPR-2024/3535
M4LW-24OR0402029

Materials Science and Technology Division
Nuclear Energy and Fuel Cycle Division

ANALYSIS OF DEFORMATION AND FRACTURE MECHANISMS IN FRICTION STIR WELDING ON NEUTRON-IRRADIATED 304L STAINLESS STEEL

S. Kang
W. Tang
X. Chen
M. N. Gussev

August 2024

Prepared by
OAK RIDGE NATIONAL LABORATORY
Oak Ridge, TN 37831-6079
managed by
UT-BATTELLE, LLC
for the
U.S. DEPARTMENT OF ENERGY
under contract DE-AC05-00OR22725

CONTENTS

LIST OF FIGURES

LIST OF TABLES

ABBREVIATIONS

appm	atomic parts per million
EBSD	electron backscatter diffraction
FSW	friction stir welding
HAZ	heat-affected zone
IPF	inverse pole figure
IQ	image quality
NPP	nuclear power plant
ROI	region of interest
SEM	scanning electron microscopy
SS	stainless steel
SZ	stir zone
TA	top advancing
TMAZ	thermomechanical-affected zone
TR	top retreating
TS	top stir zone

ACKNOWLEDGMENT

The research was sponsored by the US Department of Energy Office of Nuclear Energy's Light Water Reactor Sustainability Program Materials Research Pathway under contract DE-AC05-00OR22725 with UT Battelle LLC/Oak Ridge National Laboratory and collaboration from the Electric Power Research Institute.

The authors would like to acknowledge the people and teams who worked on the weldment production and irradiated specimen transportation, handling, and preparation, including Oak Ridge National Laboratory's Radiochemical Engineering Development Center, Irradiated Material Examination and Testing, and Low Activation Materials Development and Analysis facilities, Oak Ridge National Laboratory's Materials Joining Group, and the Electric Power Research Institute.

EXECUTIVE SUMMARY

This report presents recent experimental findings on the deformation behavior and fracture mechanisms of friction stir welded miniature specimens fabricated from neutron-irradiated 304L stainless steel containing He (estimated He concentration of 10 atomic parts per million). Mechanical testing was conducted using a scanning electron microscope with an electron backscatter diffraction detector.
The study demonstrated that tensile specimens from various metallurgical zones maintained structural integrity throughout the mechanical tests. No sudden fractures or severe cracking were observed.
scanning electron microscopy/electron backscatter diffraction data revealed typical deformation processes for austenitic steel, including lattice rotation, slip line formation and evolution, and strain-induced twinning. Minor fracture events at the grain or subgrain level were deemed insignificant.
These results indicate that friction stir welding (FSW) can produce mechanically robust welds, free from macroscopic cracks (e.g., on the scale of millimeters) even in irradiated austenitic steel with ~10 appm He. Furthermore, additional R&D efforts are needed to solve a reported FSW issue, and it was possibly related with the current FSW machine system design.

1. INTRODUCTION

In a nuclear power plant (NPP), structural components are exposed to harsh environments characterized by the combined effect of radiation, high pressure, and elevated temperatures. These conditions can lead to the degradation of materials, necessitating the repair or replacement of certain parts or components. Repairing irradiated NPP components faces one specific issue: the presence of transmuted He. Because stainless steels (SSs), which are commonly used in nuclear reactors, contain Ni and impurity B, He accumulation under irradiation is impossible to avoid. The B and Ni transmute into He via the following reactions:

$$^{10}\mathrm{B} + \mathrm{n} \rightarrow {}^{7}\mathrm{Li} + {}^{4}\mathrm{He} \quad (1)$$

$$^{58}\mathrm{Ni} + \mathrm{n} \rightarrow {}^{59}\mathrm{Ni} + \gamma \quad (2)$$

$$^{59}\mathrm{Ni} + \mathrm{n} \rightarrow {}^{56}\mathrm{Fe} + {}^{4}\mathrm{He} \quad (3)$$

Helium is insoluble in steel. Under fusion welding, the insoluble He migrates at material grain boundaries and causes grain boundary embrittlement. Meanwhile, with the local transient elevated temperature in fusion welding, tensile thermal stress appears in the fusion zone and heat-affected zone (HAZ). Therefore, He-induced cracking always occurs in the HAZ or fusion zone when fusion welding is applied on irradiated steels. An example of He-induced cracking after fusion welding is illustrated in Figure 1 [1], with 8.3 atomic parts per million (appm) of He in the material. The two key factors contributing to He-induced cracking are the elevated temperature and tensile stress [2].

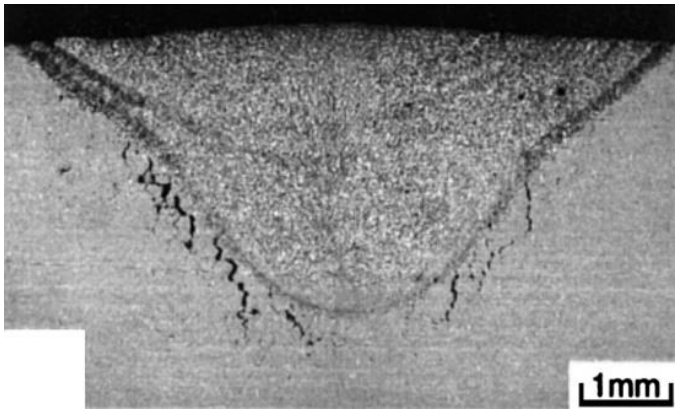

Figure 1. He-induced cracks in the weld HAZ of SS containing 8.3 appm He [1]. Note that many cracks exceed 1 mm in length, and the total length of macroscopic cracks is well above ~5–6 mm.

Friction stir welding (FSW) is a solid-state material joining technique. It joins materials through plastic deformation and recrystallization at peak temperatures significantly below the materials' melting points. The FSW's low peak temperatures associated with FSW make it a promising method for He content materials joining and processing, such as irradiated components from NPPs. Oak Ridge National Laboratory applied FSW on irradiated 304L SS in the past and published preliminary study results [3, 4]. This report addresses in-depth characterization and analysis of the deformation and fracture mechanisms of the FSW containing approximately 10 appm He.

2. MATERIALS AND EXPERIMENTAL METHODS

2.1 CUSTOM 304L STAINLESS STEEL AND TEST MATRIX

Coupons of custom 304L SS heats were irradiated with neutrons in the High Flux Isotope Reactor for three cycles (22–26 days per cycle) in 2014 [5]. The heats varied in B amount to get different He content after irradiation [5]. The present work focused on FSW made with heat D with an estimated 10 appm He [5]. Miniature tensile specimens were extracted from the heat D FSW coupon (ID: 304D-5-14) using electrical discharge machining [4]. The microstructure specimens from the 304D-5-14 coupon were characterized earlier using scanning electron microscopy (SEM)/electron backscatter diffraction (EBSD); the results showed He-induced features such as He bubble clusters, or "clouds," forming large bubbles or pores [4]. **Table 1** shows the specimen list and test matrix used in this study. Three miniature specimens from different metallurgical zones (TA is "top advancing," TR is "top retreating," and TS is "top stir zone") of the 304D-5-14 FSW coupon were tested to elucidate the deformation mechanisms and fracture characteristics.

Table 1. Test matrix

ID	Specimen location	Reached strain level (at the end of the mechanical test)
304D-5-14-TA2	Advancing side thermomechanical-affected zone/HAZ	0.7
304D-5-14-TS2	Stir zone	0.55
304D-5-14-TR2	Retreating side thermomechanical-affected zone/HAZ	0.3

2.2 IN SITU MECHANICAL TEST WITH ELECTRON BACKSCATTER DIFFRACTION

In situ mechanical testing with EBSD was used in this study to observe deformation mechanisms. The advantage of this technique is its capability to track the deformation at the region of interest (ROI). Figure 2(a) shows the in situ mechanical test apparatus with the tensile stage installed in the pretilt holder. Figure 2(b) shows the interior of the SEM chamber showing the EBSD camera and 70° pretilted tensile specimen. A few ROIs were selected for EBSD in the gauge section of the samples. The ROI is the area used for collecting the EBSD pattern; usually, 3–4 areas are selected along the sample gauge. The mechanical test was interrupted, and the EBSD scan was performed at the same ROI to track the deformation mechanisms throughout the test.

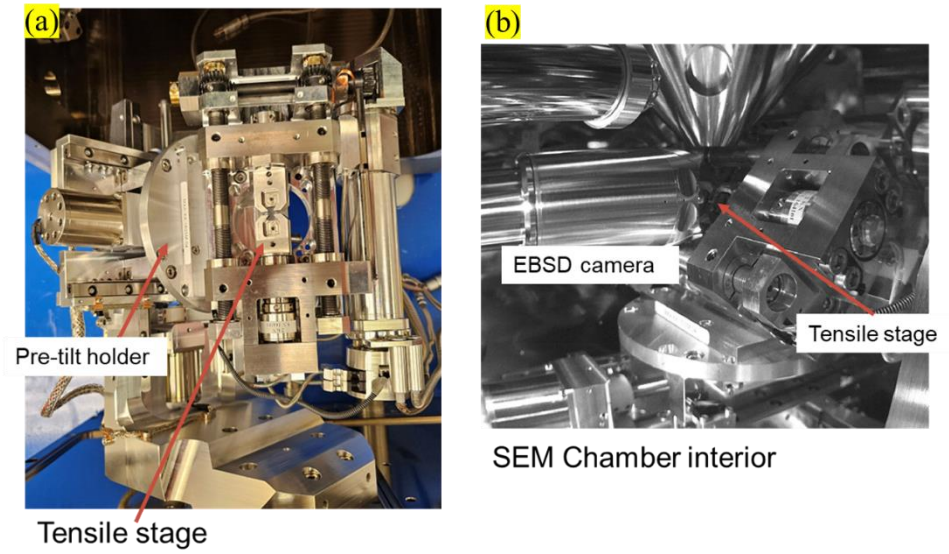

Figure 2. (a) In situ mechanical test apparatus including tensile stage and pretilt holder and (b) SEM chamber interior with tensile stage and EBSD camera.

3. RESULTS AND DISCUSSION

3.1 DEFORMATION MECHANISMS IN SPECIMENS CUT FROM DIFFERENT METALLURGICAL ZONES

3.1.1 304D-5-14 TA2 Specimen

Specimen 304D-5-14-TA2 was extracted from the FSW thermomechanical-affected zone (TMAZ)/HAZ areas on the advancing side, and its gauge contained both TMAZ and HAZ, as shown in Figure 3. In the HAZ (left side), larger equiaxed grains with a size of a few hundred micrometers were observed. Additionally, annealing twins were observed inside of a grain showing different colors of twin lamella. As the observing location moved toward the TMAZ area (right side), grain sizes reduced, and grains deformed and elongated because of plastic strain during the FSW process.

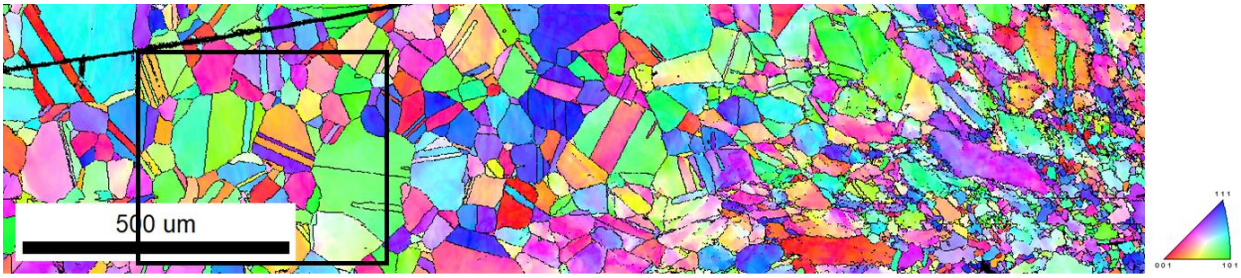

Figure 3. EBSD inverse pole figure at the gauge area along the tensile direction of 304D-5-14-TA2 TMAZ/HAZ specimen. Black box is the scanned area in Figure 5. The color key at the bottom right is universal for all inverse pole figure images in this report.

Figure 4 shows the tensile curve for the 304D-5-14-TA2 specimen with deformation steps marked as [S01]–[S05] and SEM images taken at different steps. The figure shows that as the strain level (i.e., step) increased, the surface morphology changed from a smooth electropolished surface to a rough surface. Multiple features appear, such as slip lines in grains. Lattice rotation generated a fairly rough surface,

shown in Figure 4d; however, no obvious cracks appear, suggesting limited or no He-induced embrittlement.

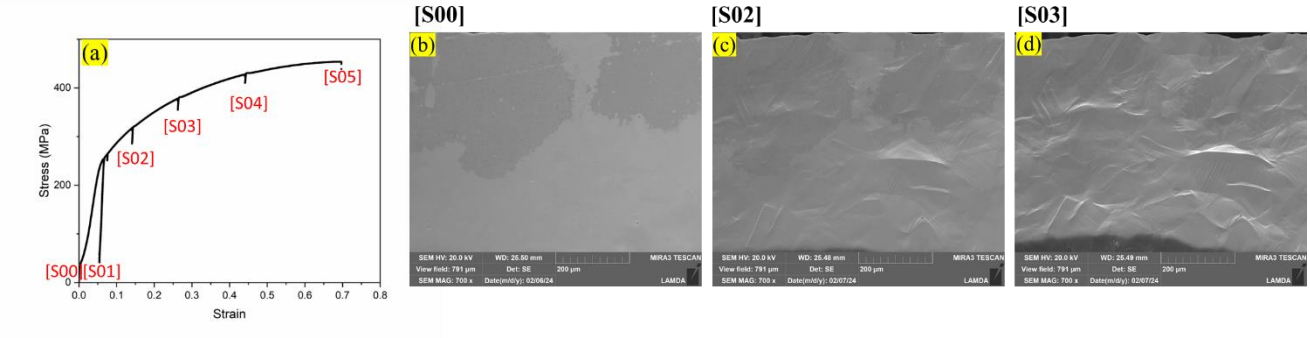

Figure 4. 304D-5-14-TA2 (a) stress–strain curve from the tensile test and SEM images at each step: (b) [S00], (c) [S02], and (d) [S03].

Figure 5(a–f) shows the image quality (IQ) and inverse pole figure (IPF) maps of the 304D-5-14-TA2 sample recorded at different step (i.e., strain) levels. At [S00], preexisting twins were observed in the IQ map (Figure 5a) and IPF maps (Figure 5d–f). As the step increased, the IQ degraded because of the defects and generation of slip lines. The deformation-induced twinning started to be observed in a grain at [S02]. Then at [S03], the twinning grew, and new twinning was formed nearby the existing twinning.

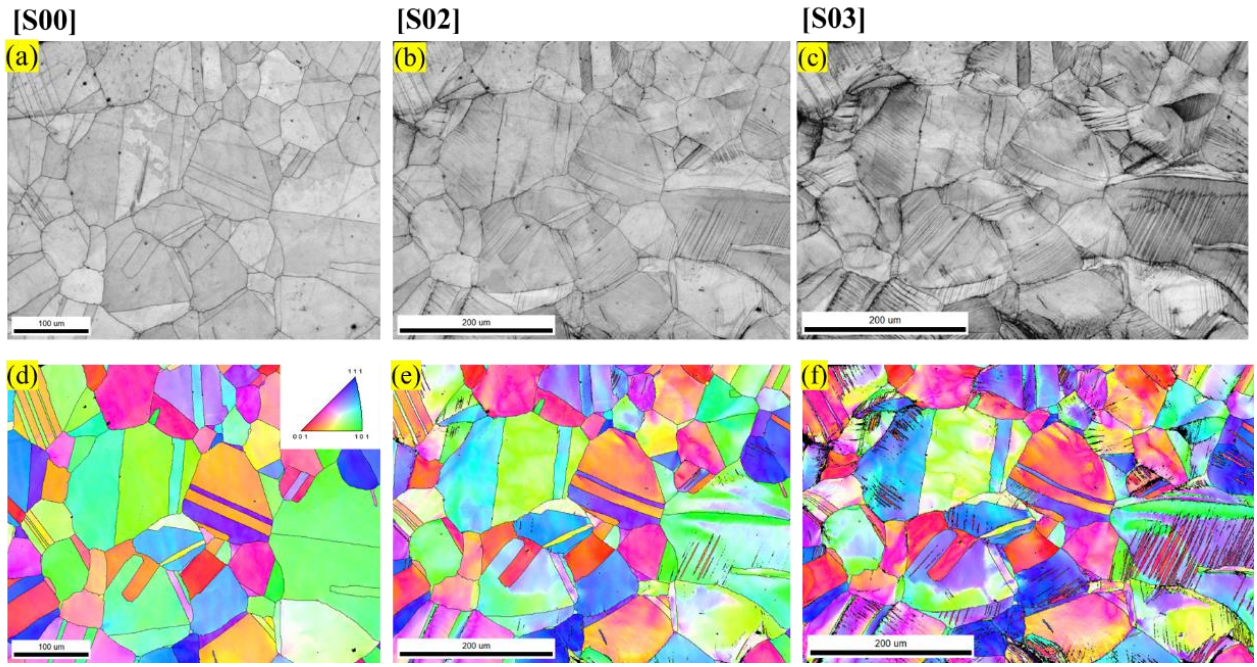

Figure 5. EBSD analysis of 304D-5-14-TA2 with the steps [S00], [S02], and [S03]: (a–c) IQ and (d–f) IPF.

Overall, the SEM/EBSD observation showed usual annealed or cold-deformed steel deformation in the FSW TMAZ/HAZ area. No specific or detrimental features, such as early shear bands, crack opening, and more, were spotted.

3.1.2 304D-5-14-TS2 Specimen

The 304D-5-14-TS2 sample, shown in Figure 6, was cut from the center of the stir zone (SZ), presenting an interesting microstructure of equiaxed, partially recrystallized grains with an average grain size of approximately 10 μm.

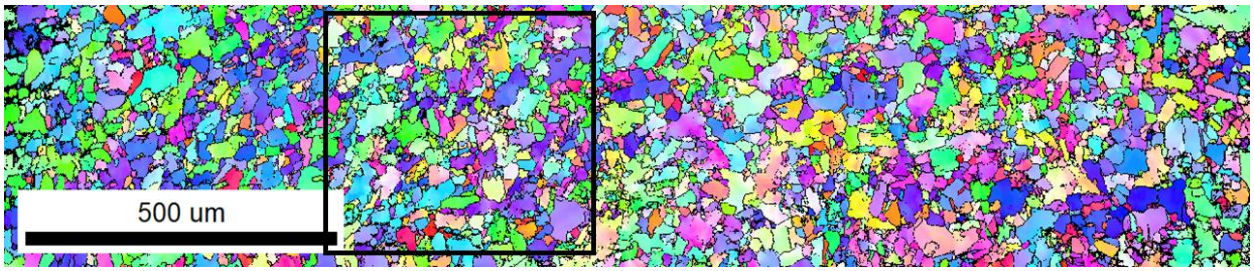

Figure 6. EBSD IPF along the tensile direction of the 304D-5-14-TS2 SZ specimen. Black box is the scanned area in Figure 8.

Figure 7 shows the stress–strain curve of the 304D-5-14-TS2 specimen. The overall trend was similar to 304-5-14-TA2, in which the surface deformation developed and surface roughness increased with increasing the strain level. Single slip lines were difficult to see in this sample, possibly because of the smaller equiaxed grain size. A future study may investigate the effect of grain size on slip dynamics. The previous research [6] showed that grain size affected slip dynamics such as slip velocity.

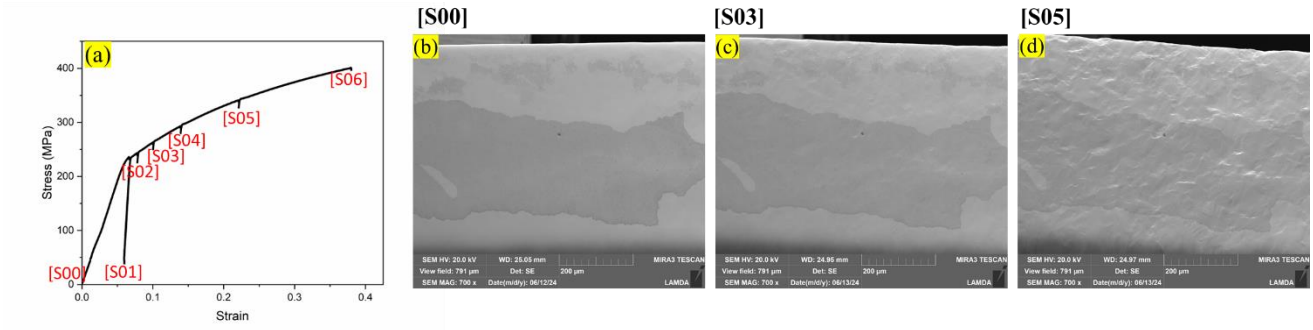

Figure 7. 304D-5-14 TS2 (a) stress–strain curve from the tensile test and SEM images at each step: (b) [S00], (c) [S03], and (d) [S05].

Microstructure evolution, shown in Figure 8, was typical for the austenitic alloy; no specific features could be attributed to He-induced degradation. Figure 8(a–f) shows the IQ and IPF maps of the 304D-5-14-TS2 sample depending on the step (i.e., strain). As the step increased, the IQ degraded because of the defects (i.e., grain boundary, slip lines) during plastic deformation. At [S05], twinning was observed but grew less than the TA2 at the similar strain level (~0.2). Grain size might affect the formation of the twinning.

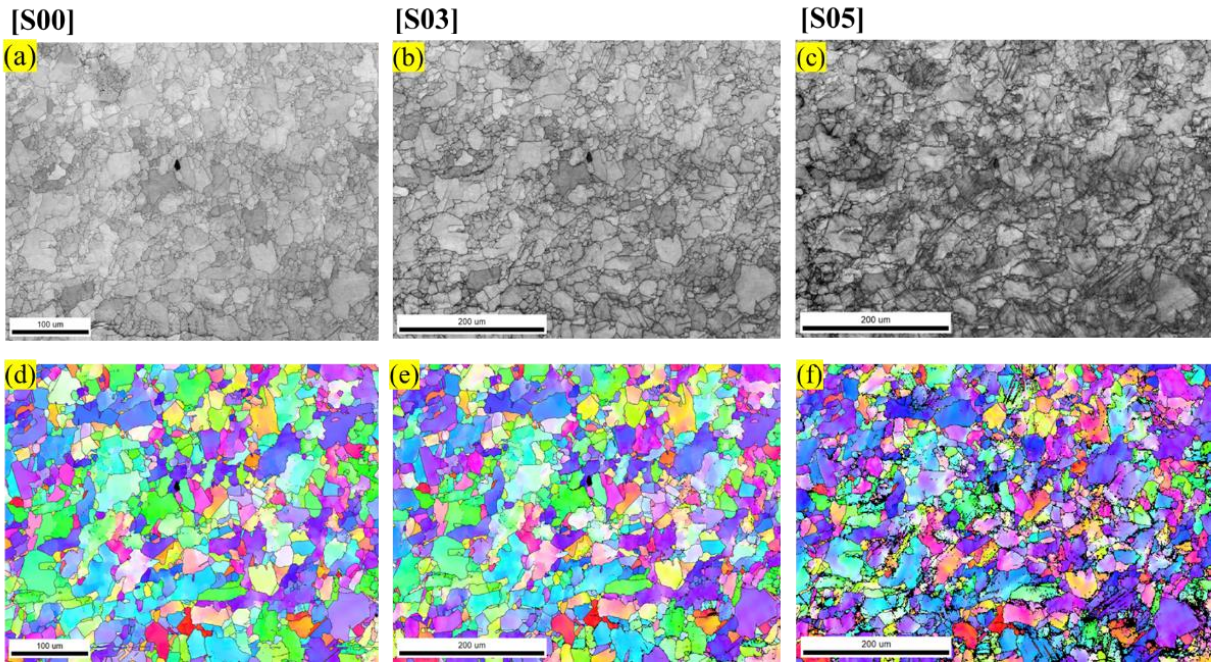

Figure 8. EBSD analysis of 304D-5-14-TS2 with the steps (a, d) [S00], (b, e) [S03], and (c, f) [S05]. (a–c) IQ and (d–f) IPF.

3.1.3 304D-5-14-TR2 Specimen

The 304D-5-14-TR2 sample shown in Figure 9 was extracted from the TMAZ/HAZ area on the retreating side. Compared with the TMAZ/HAZ specimen on the advancing side (304D-5-14-TA2), this specimen contained wider TMAZ and may have contained part of the SZ (left side with smaller equiaxed grains).

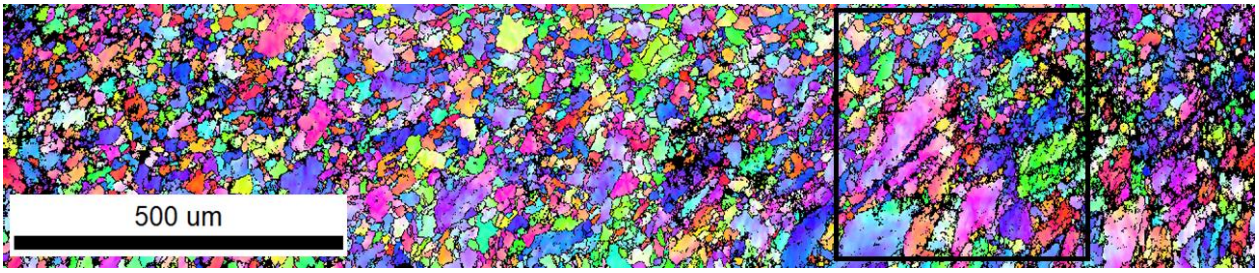

Figure 9. EBSD IPF along the tensile direction of 304D-5-14-TR2 TMAZ/HAZ specimen. Black box is the scanned area in Figure 11.

Figure 10 shows the stress–strain curve of 304D-5-14-TR2. The tendency of surface deformation resembles that of the 304D-5-14-TA2. The slip lines and grain boundaries were observed as the step increased.

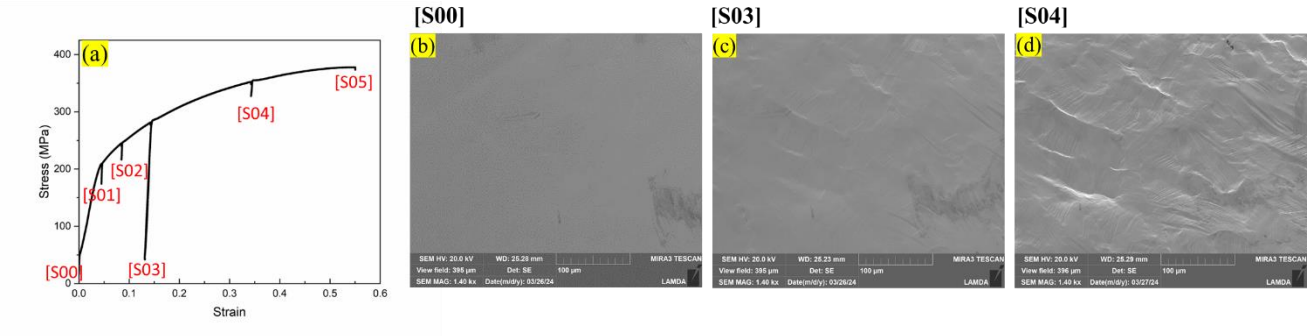

Figure 10. 304D-5-14 TR2 (a) stress–strain curve from the tensile test and SEM images at each step: (b) [S00], (c) [S03], and (d) [S04].

Figure 11(a–f) shows the IQ and IPF maps of the 304D-5-14-TR2 sample depending on the step (i.e., strain). These maps were scanned at the TMAZ showing elongated or deformed grains. In the figure at [S04] with a strain level of approximately 0.4, the IPF color changes mostly to red and blue, indicating the grain orientation changed toward (001) and (111), as shown in Figure 11(f). Also, the deformation-induced twinning was mostly observed in a grain at [S03] with an equivalent strain of approximately 0.1. The twinning was mostly observed at bigger grains, so it would be interesting to study the grain size effect on the formation of the deformation twinning.

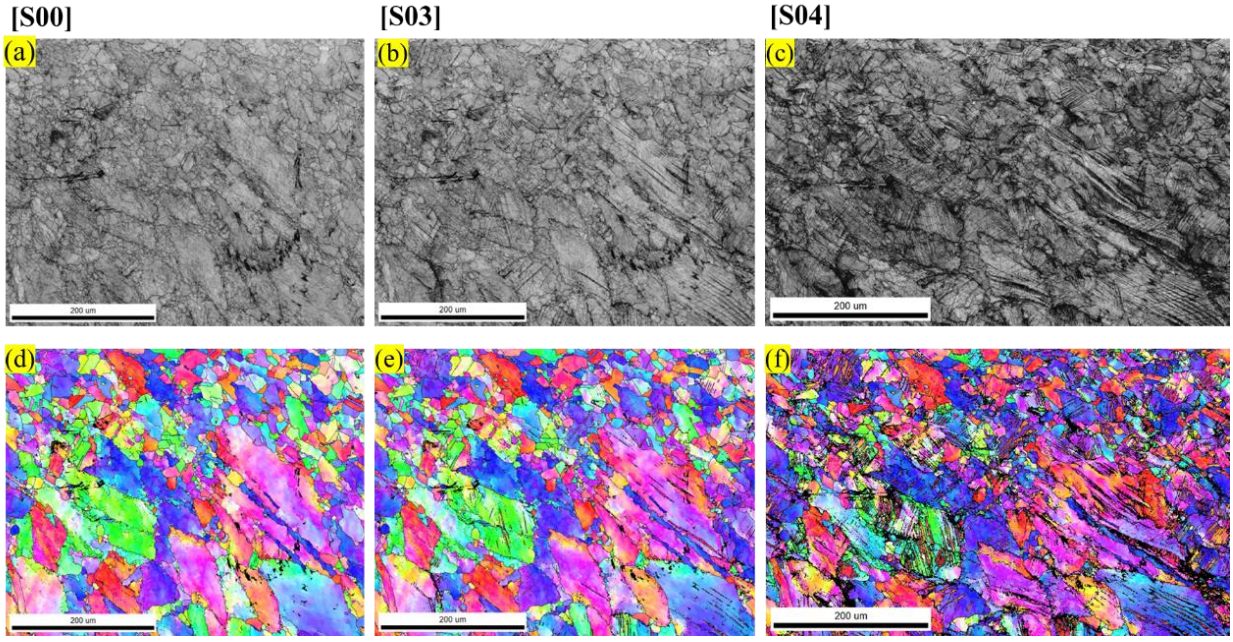

Figure 11. EBSD analysis of 304D-5-14 TR2 with steps [S00], [S03], and [S04]: (a–c) IQ and (d–f) IPF.

Overall, no obvious He-induced embrittlement was observed. All three specimens tested showed reasonable ductility and active deformation mechanisms typical for irradiated austenite.

3.2 FRACTURE MECHANISMS AT DIFFERENT FRICTION STIR WELDING ZONES

Figure 12(a–c) shows three sample gauges at the last step during in situ mechanical tests. For the TA2 sample, small cracks (~50 μm) were observed at the gauge edge in the last step [S05], corresponding to a strain of about 0.6. No catastrophic failure was observed even at 60% of the deformation. Figure 13(a) shows the magnified images of cracks at the edge of [S05]. Moreover, microcracks were observed with high magnification; Figure 13(b–d) shows the microcrack of [S05] in the IQ and IPF maps. The size of the microcrack was around 5 μm and was located at the grain boundary triple junction based on EBSD data.

For the TS2 specimen, no crack was observed at [S06], corresponding to strain of approximately 0.38 based on the gauge scan at the last step, as shown in Figure 12(b).

Figure 12(c) shows cracks at the gauge edge of the TR2 sample at step [S05], corresponding to a strain level of approximately 0.55. Figure 14(a) shows the magnified crack image at the edge. The crack length was approximately 40 μm, which was around 6% of the specimen width. No catastrophic crack was observed even around 55% deformation. Figure 14(b–d) shows a microcrack observed at [S05] with IQ and IPF maps of the TR2 specimen. The microcrack was around 10 μm and nucleated at the grain boundaries. The grains nearby the microcrack contained the twinning. The interaction between grain boundaries and twinning will be interesting to study in the future.

Although up to 50 μm microcracks were observed from FSW specimens with approximately10 appm He, no catastrophic failure was observed at higher strain (>0.38), which shows the good integrity of FSW as a repair technique for NPPs.

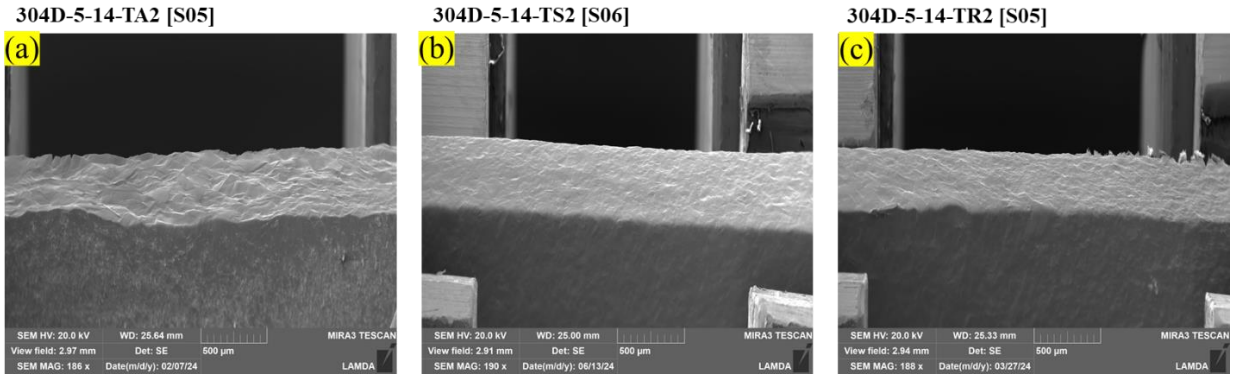

Figure 12. Crack images at the last step of in situ tensile tests: (a) 304D-5-14-TA2, (b) 304D-5-14-TS2, and (c) 304D-5-14-TR2.

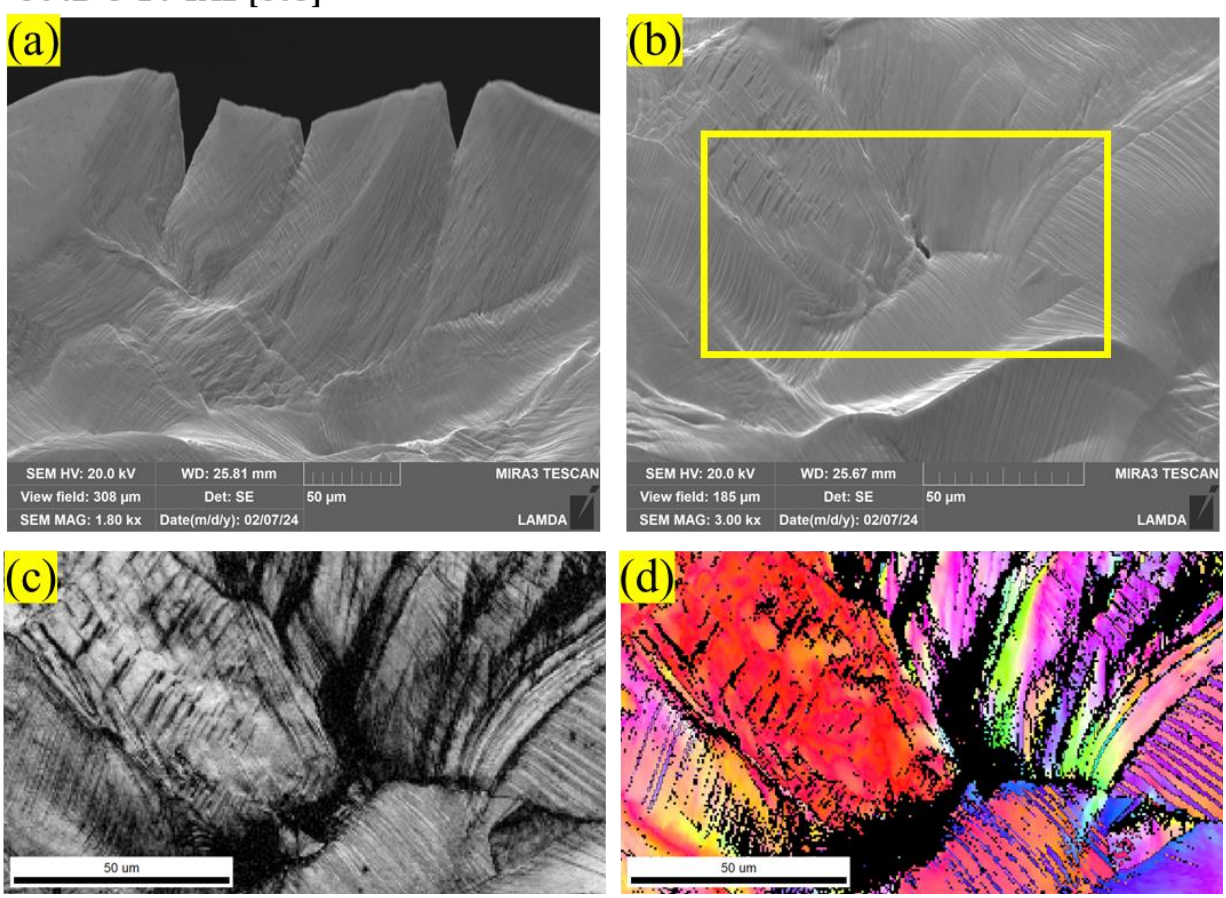

Figure 13. 304D-5-14-TA2 (a) high-magnification crack image on the edge of the sample, (b) microcrack image on the surface of the sample, (c) IQ map from the yellow box in (b), and (d) IPF map from the yellow box in (b).

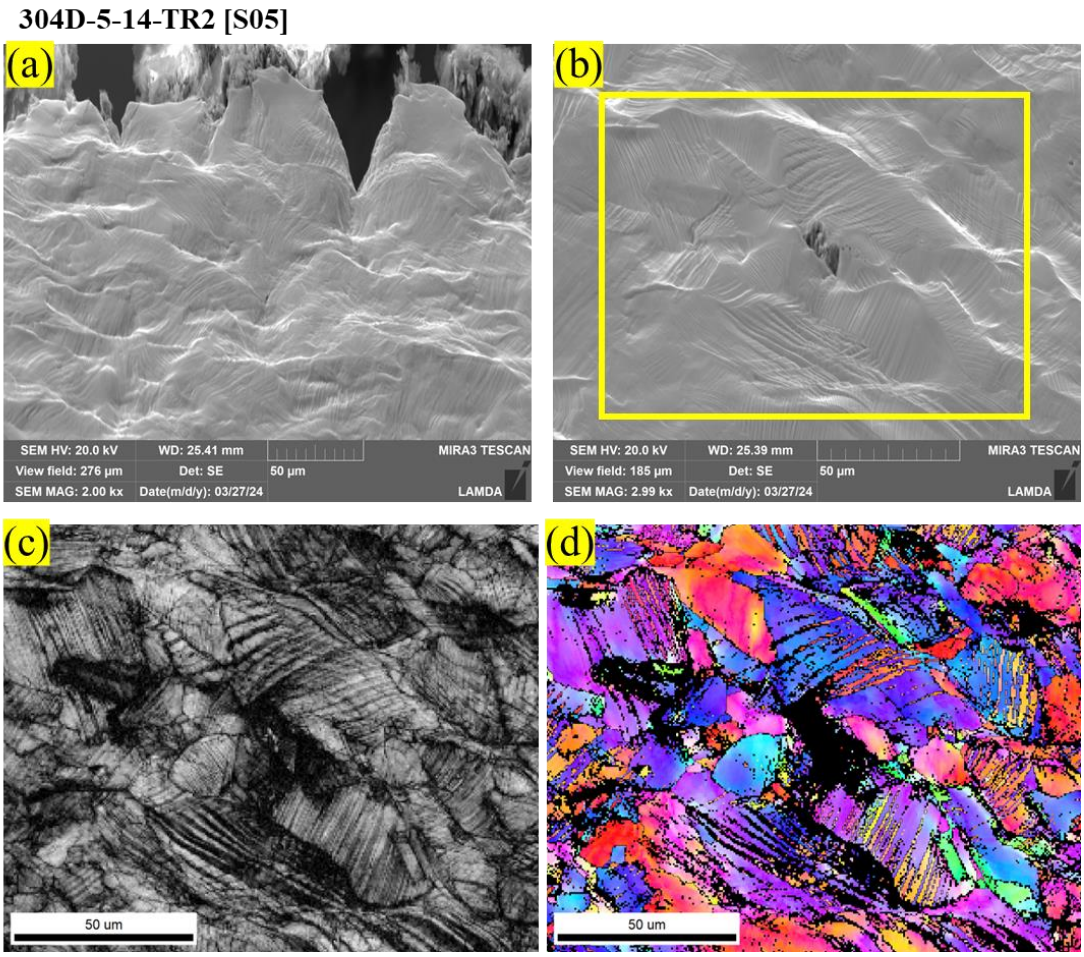

Figure 14. 304D-5-14-TR2 (a) high-magnification crack image on the edge of the sample, (b) microcrack image on the surface of the sample, (c) IQ map from the yellow box in (b), and (d) IPF map from the yellow box in (b).

4. CONCLUSIONS AND FUTURE WORK

This study focused on the mechanical performance and fracture behavior of an irradiated 304L SS FSW specimen containing ~10 appm He. Various metallurgical zones, including the SZ, TMAZ, and HAZ on both the advancing and retreating sides of the weld, were evaluated.

Defects such as grain boundary, slip lines, and twinning were observed during in situ mechanical tests. Future work is suggested based on the result in this study of observed twinning in some grains, which may vary by grain size.

A limited number of microcracks (~50 µm) were observed at the edges of the samples from the TMAZ/HAZ when strain levels exceeded 0.5. Despite this cracking, the overall ductility remained high with no tendency toward catastrophic brittle failure. The generalized results indicate that FSW with ~10 appm He maintains good mechanical integrity. It is worth to note that a surface defect was formed at the end of the friction stir weld, mainly in the unirradiated run-off 304L SS tab [7]. The reason of such defect formation is undetermined but likely related with the FSW machine system design: inconstant rigidity along the FSW path. Further R&D efforts are needed to eliminate the end weld surface defect.

5. REFERENCES

[1] K. Asano, S. Nishimura, Y. Saito, H. Sakamoto, Y. Yamada, T. Kato, T. Hashimoto, Weldability of neutron irradiated austenitic stainless steels, Journal of Nuclear Materials 264(1-2) (1999) 1-9.
[2] S. Kawano, F. Kano, C. Kinoshita, A. Hasegawa, K. Abe, Effect of weld thermal cycle, stress and helium content on helium bubble formation in stainless steels, Journal of nuclear materials 307 (2002) 327-330.
[3] M. Gussev, W. Tang, N. Bibhanshu, T. Rosseel, Microstructure and Mechanical Performance of the Friction Stir Welds Performed on Neutron-Irradiated Steel with Helium, Oak Ridge National Laboratory, 2021.
[4] W. Tang, M. Gussev, T. Rosseel, X. Chen, Comprehensive characterization of helium-induced degradation of the friction stir weld on neutron-irradiated 304L Stainless Steel, M3LW-23OR0406013 Oak Ridge National Laboratory, 2023.
[5] Zhili Feng, Nesrin Cetiner, Roger Miller, G. Frederick, Completion of the first batch of irradiation experiments to produce helium-containing SS304 samples for use in development of weld repair techniques., M3LW-14OR0406014, Oak Ridge National Laboratory, 2014.
[6] J. Randolph-Flagg, J.E. Reber, Effect of grain size and grain size distribution on slip dynamics: An experimental analysis, Tectonophysics 774 (2020) 228288.
[7] Zhili Feng, Roger Miller, Jian Chen, Wei Tang, Scarlett Clark, Brian Gibson, Mark Vance, Gregory Frederick, Jonathan Tatman, B. Sutton, Complete Report on the Development of Welding Parameters for Irradiated Materials, ORNL/SPR-2017/568, Oak Ridge National Laboratory, 2017.